Supplementary Materials for "Dynamic failure mechanisms of an urban sinkhole collapse revealed by dense near-field seismic observations"

Tae-Kyung Hong[1*], Byeongwoo Kim[1], Seongjun Park[1], Jeongin Lee[1], and Junhyung Lee[1]

Affiliation and address:

[1]Yonsei University, Department of Earth System Sciences, 50 Yonsei-ro, Seodaemun-gu Seoul 03722, South Korea.

Correspondence to:

tkhong@yonsei.ac.kr (Tae-Kyung Hong)

Contents of this file

Introduction

This supporting information provides additional materials and figures.

Additional information

We apply a reference seismic velocity model for the long-period waveform inversion and waveform modeling. The reference velocity model is constructed from the 1-D velocity models in the Seoul metropolitan area (Fig. S1). The seismic waves from the sinkhole event is well observed in densely-deployed seismic networks in the Seoul metropolitan. The seismic signals are observed in distances up to 100 km (Fig. S2). The seismic wavetrains present clear major-phase arrivals (Fig. S3). In particular, Rayleigh waves are strong, presenting characteristic particle motions such as radially-polarized retrograde elliptical motions (Fig. S4).

The source mechanisms are inverted from the waveform records using the long-period waveform inversion. The inverted source mechanism for the later collapse presents a vertical compression with lateral expansion (Fig. S5(a)). Synthetic waveforms for the inverted source mechanism are compared with the observed waveforms, presenting high fitness at stations in various distances (Fig. S5(b)-(h)).

We calculate ambient-noise cross-correlation functions that yield Green's functions for the paths between stations. Rayleigh waves have characteristic velocities (Fig. S6). Also, high-frequency Rayleigh waves are sensitive to shallow structures (Fig. S7). The interstation-path Green's functions across the sinkhole site are stably retrieved from ambient-noise cross-correlations (Figs. S8 and S9).

We estimate the signal-to-noise ratios (SNRs) of stacked ambient-noise cross-correlation functions. The SNRs of daily stacked cross-correlation functions in frequency band of 0.5-1.0 Hz generally range from 2 to 6 (Fig. S10). The SNRs vary with time, indicating temporal changes in the stability of the retrieved cross-correlation functions. These variations suggest that the stacking duration should be selected considering the temporal stability of the cross-correlation functions. We further compare 5-day and 7-day stacking windows for frequency band of 1.0-2.0 Hz (Fig. S11). The results demonstrate that the 7-day stacking window yields more stable cross-correlation functions and consistently higher signal-to-noise ratios.

The optimal stacking duration is determined empirically. The stacking duration is chosen to ensure stable cross-correlation functions under the prevailing noise conditions. High-frequency ambient noise generally exhibits greater temporal variability. Thus, high-frequency data require longer stacking durations to obtain stable cross-correlation functions. The daily variation of 7-day-stacked ambient-noise cross-correlation functions in frequencies of 1.0-2.0 Hz and 2.0-4.0 Hz display weak changes over the sinkhole-event date (Figs. S12 and S13).

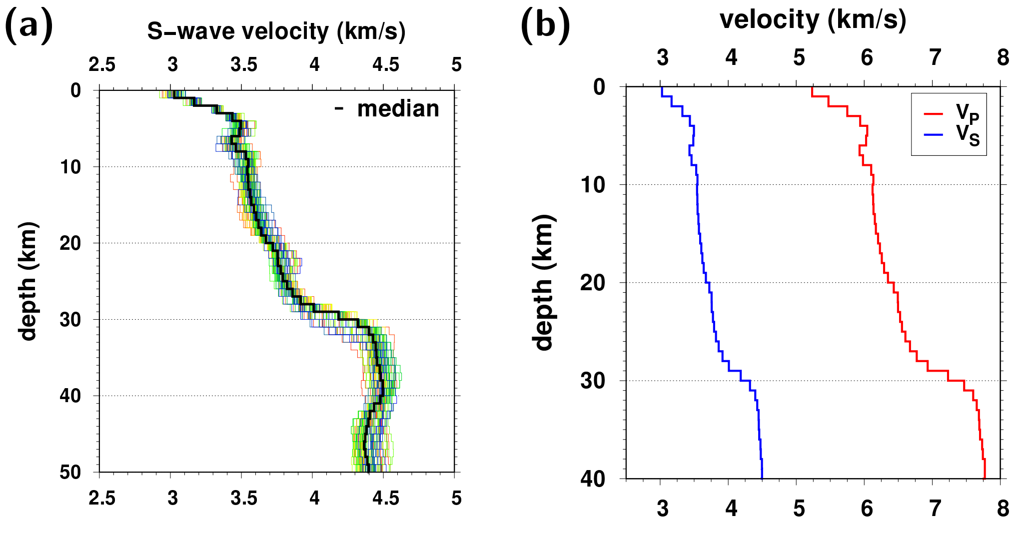

Figure S1. (a) One-dimensional P velocity models in the Seoul metropolitan area. (b) Mean 1-D P velocity model and associated S wave velocity model for V_P/V_S ratio of 1.73.

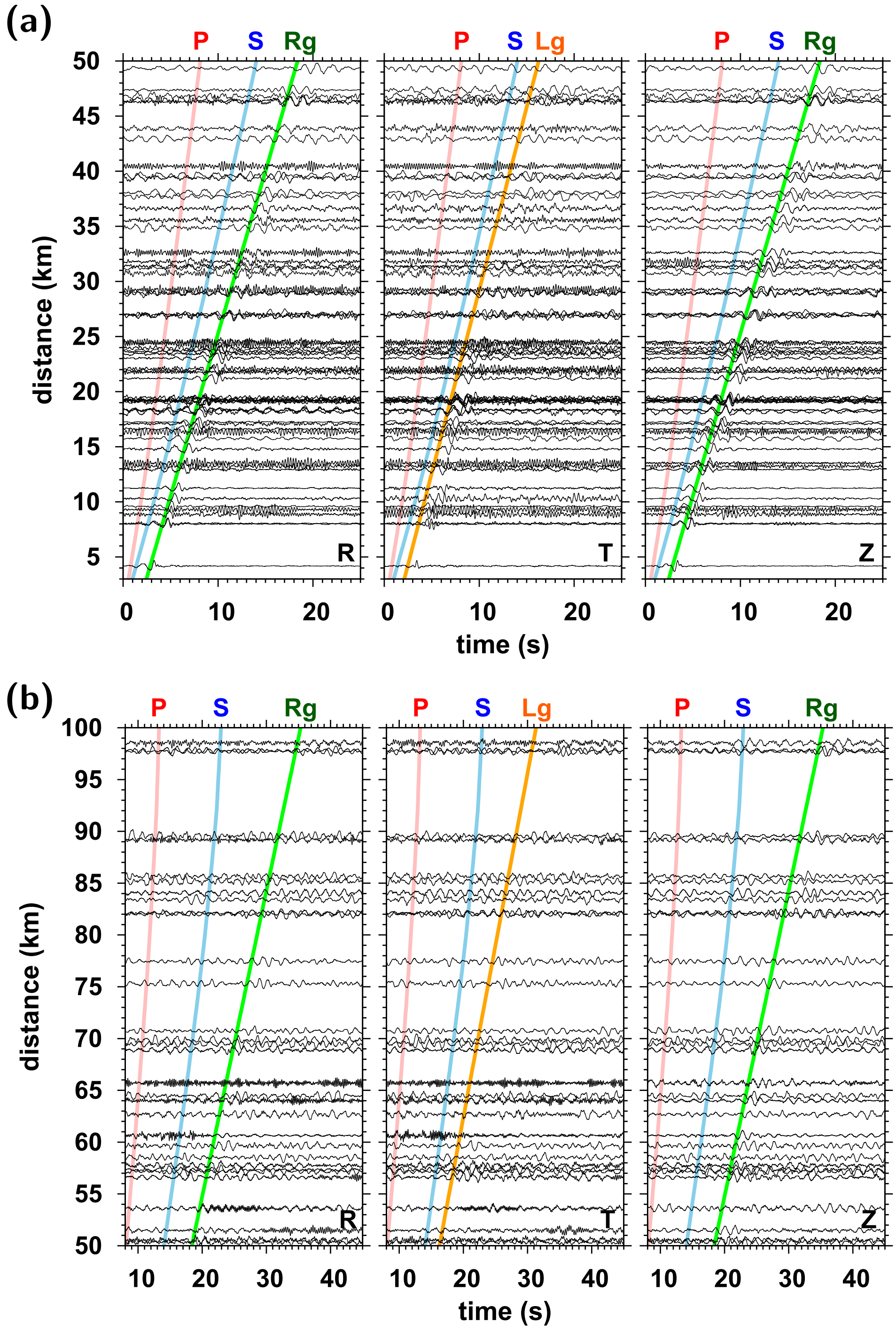

Figure S2. Three-component seismic waveform records for the sinkhole event in distances of (a) 0-50 km and (b) 50-100 km. The radial (R), tangential (T), vertical (Z) components are indicated. The traveltime curves of major phases (*P, S, Lg, Rg*) are presented (solid lines).

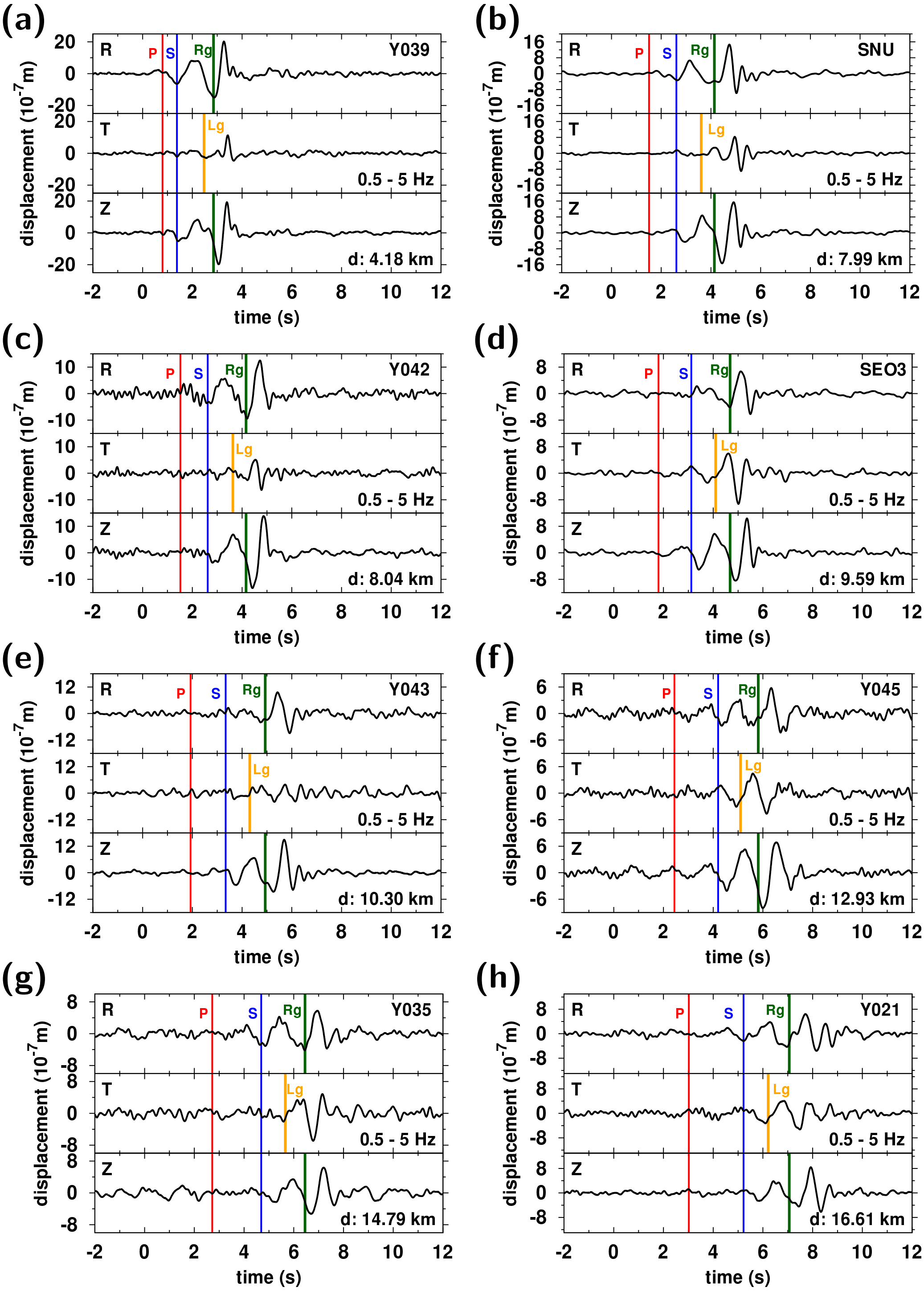

Figure S3. Three-component seismic waveform records at stations (a) Y039, (b) SNU, (c) Y042, (d) SEO3, (e) Y043, (f) Y045, (g) Y035, and (h) Y021. The seismic waveforms are bandpass-filtered between 0.5 and 5 Hz. The distances (d) are presented. The theoretical arrival times of major phases are indicated (vertical solid lines). The traveltime curves of major phases (P, S, Lg, Rg) are presented (solid lines).

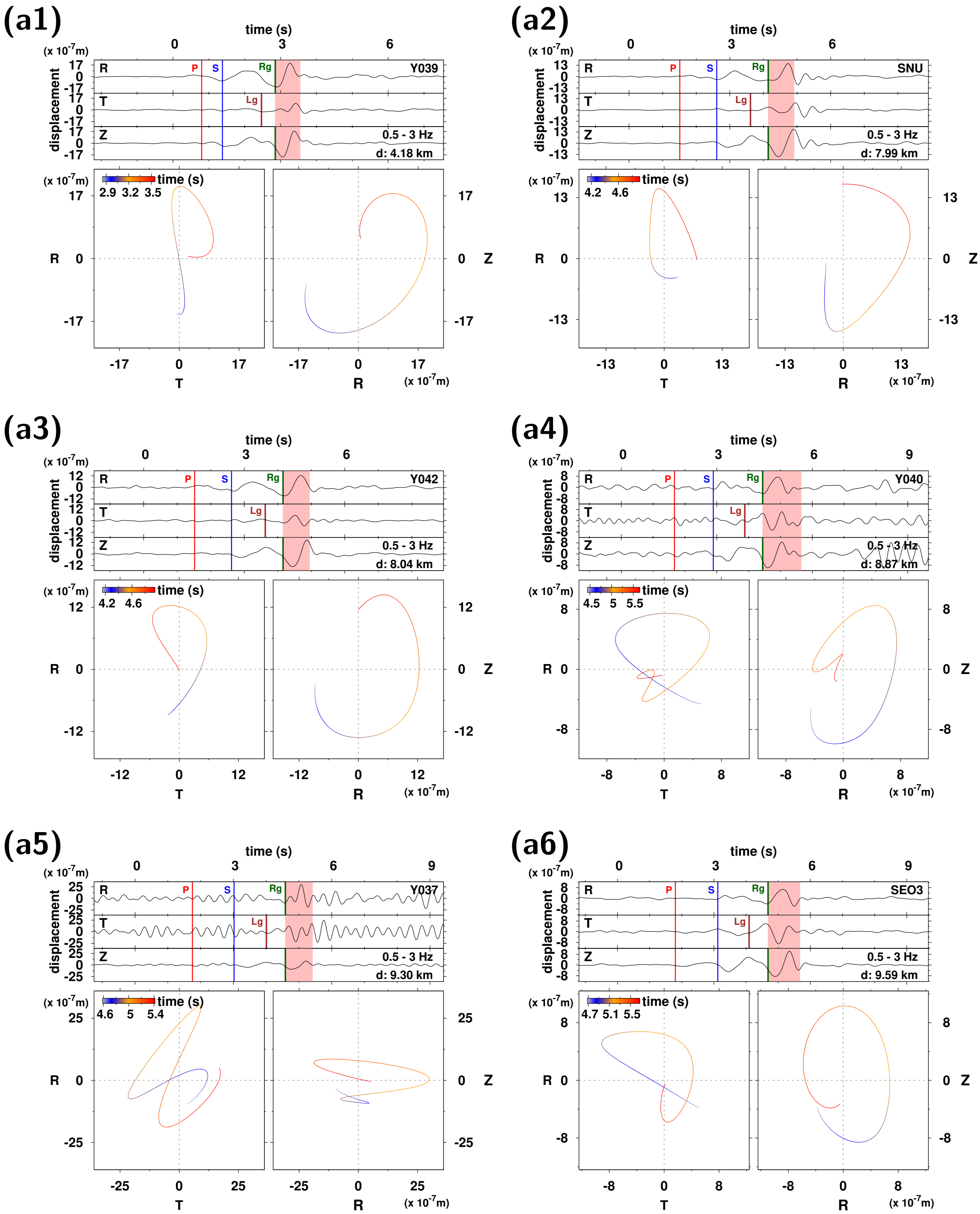

Figure S4. Three-component (R, T, Z) wavetrains and particle motions of Rayleigh waves (shaded parts in wavetrains) in frequencies of 0.5-3.0 Hz at stations in distances < 27 km: (a1) Y039, (a2) SNU, (a3) Y042, (a4) Y040, (a5) Y037, (a6) SEO3, (b1) Y043, (b2) Y053, (b3) Y045, (b4) Y032, (b5) Y038, (b6) Y035, (c1) GSGA, (c2) Y021, (c3) Y018, (c4) SWO2, (c5) Y048, (c6) YSI, (d1) Y004, (d2) Y016, (d3) Y017, (d4) SODA, (d5) Y033, (d6) Y019, (e1) Y003, (e2) Y002, (e3) Y007, (e4) Y047, (e5) Y006, (e6) Y034, (f1) Y020, (f2) INCA, (f3) Y050, (f4) Y014, (f5) Y008, and (f6) Y009. The theoretical arrival times of major phases are indicated (vertical solid lines).

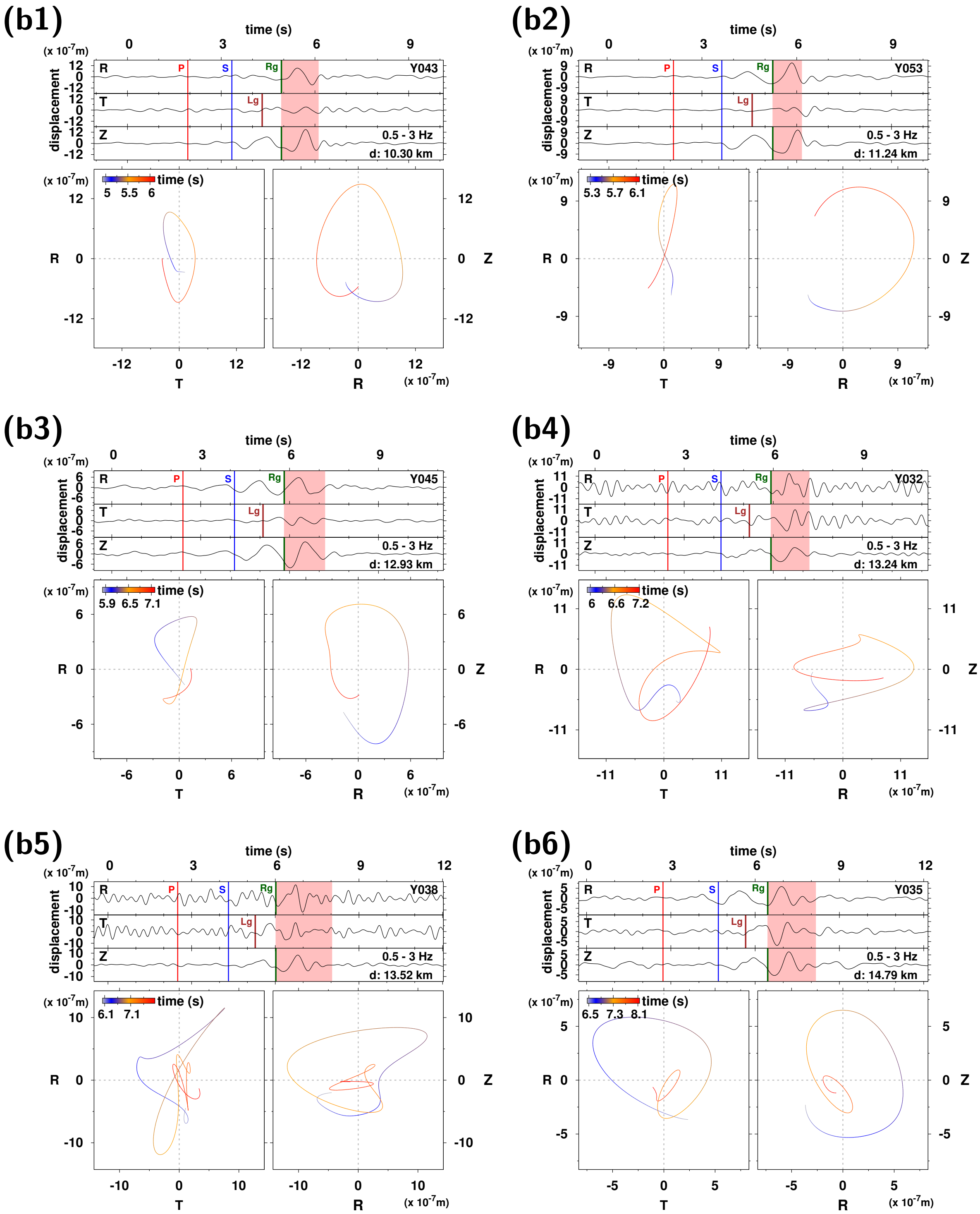

Figure S4. (continued)

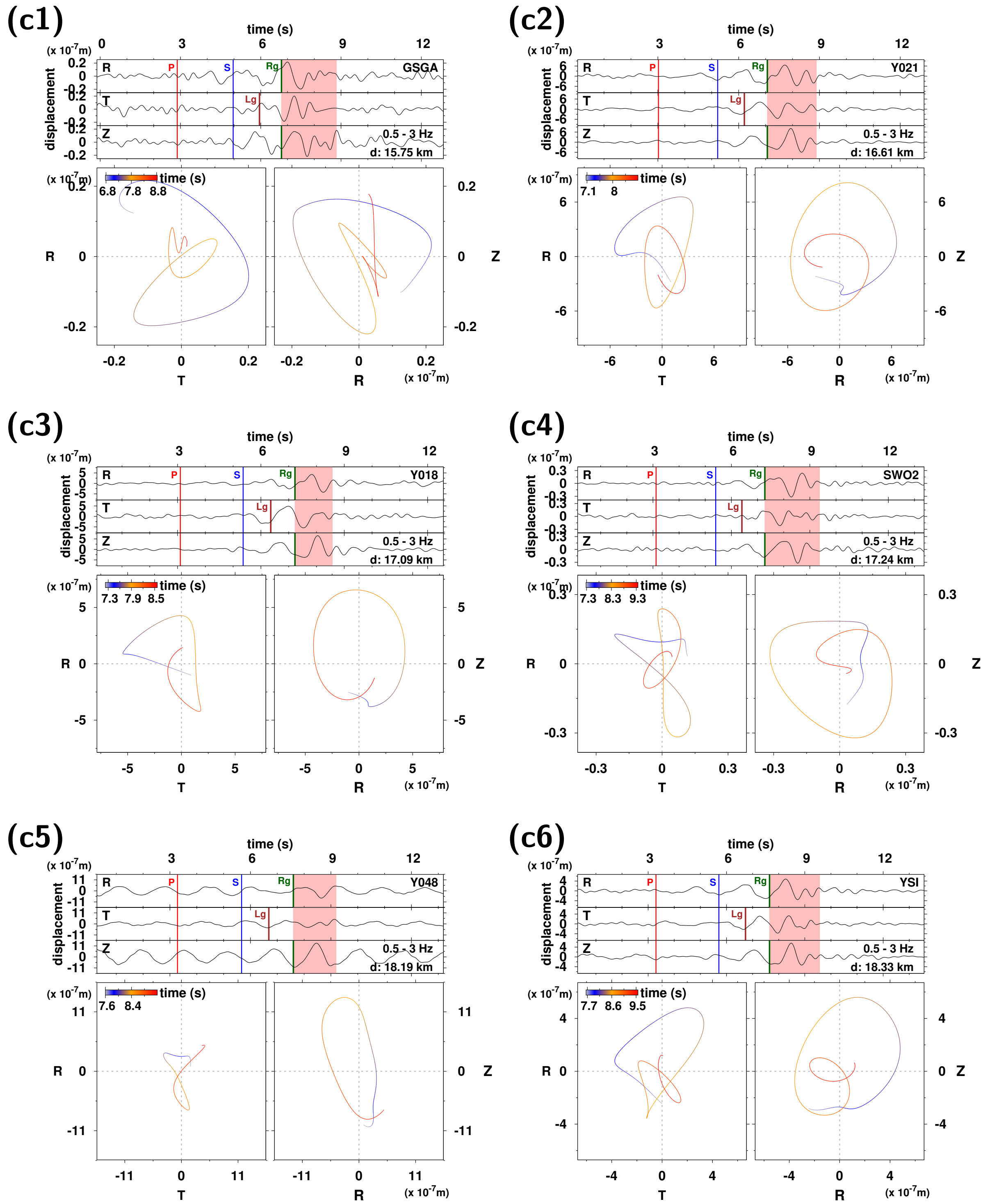

Figure S4. (continued)

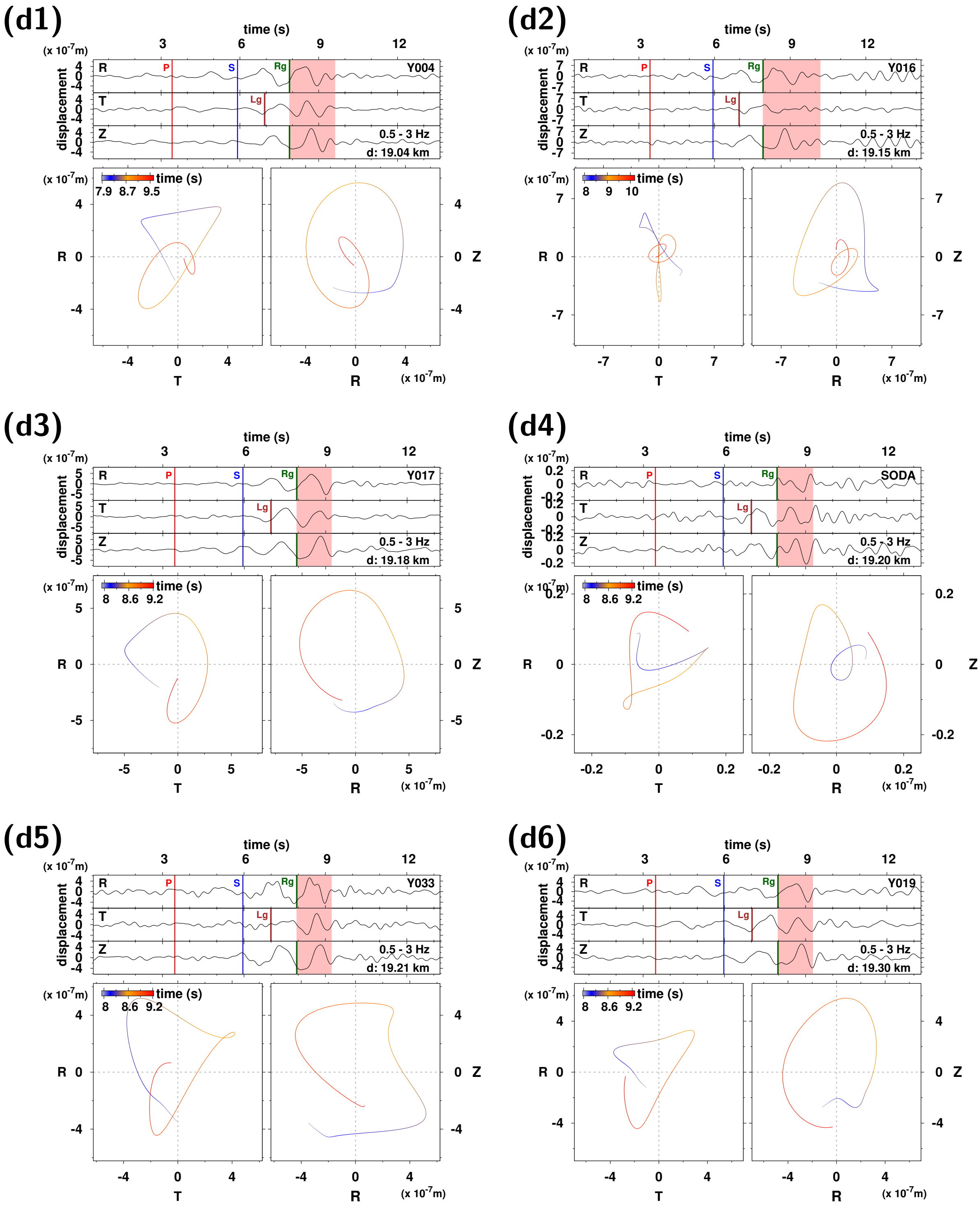

Figure S4. (continued)

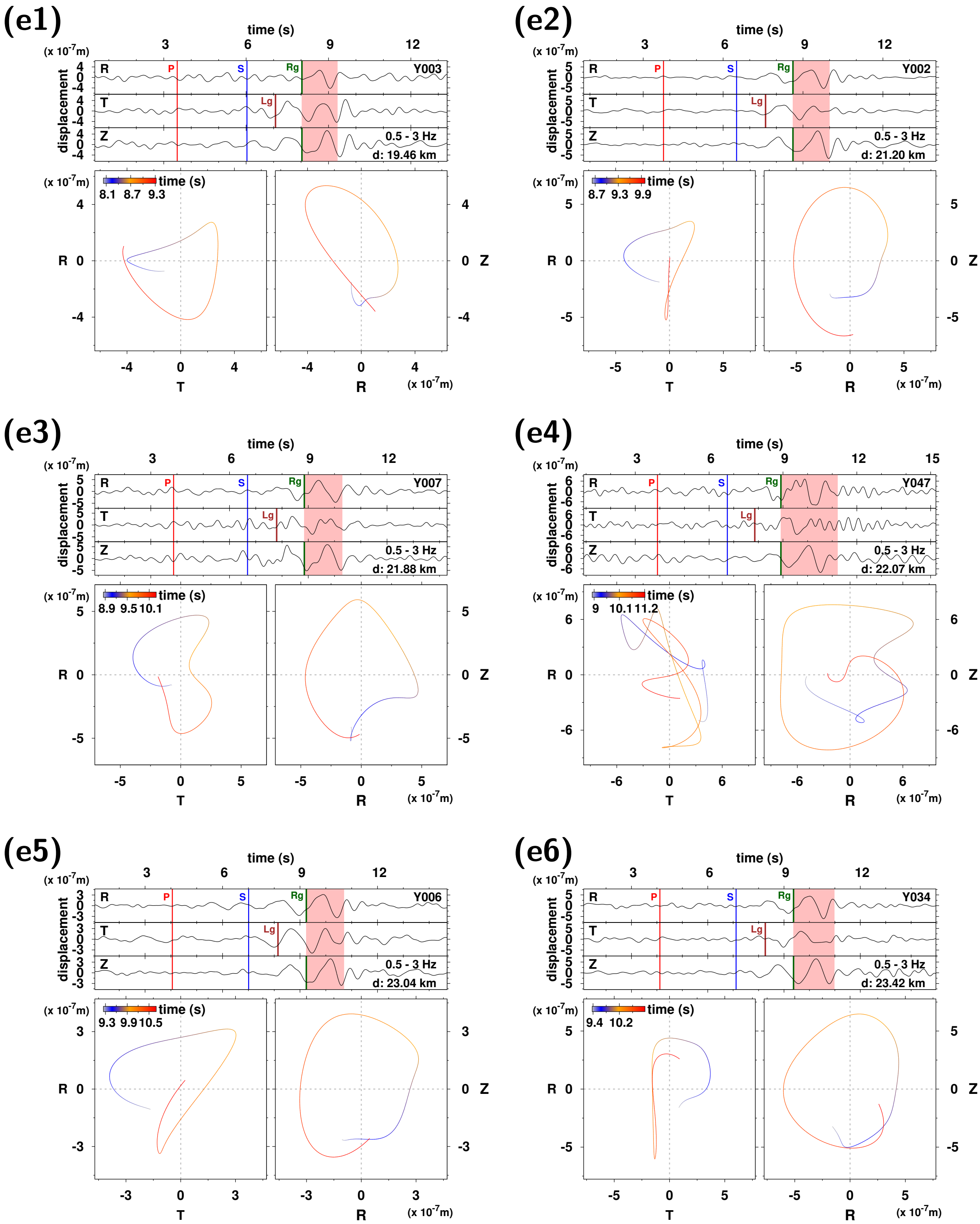

Figure S4. (continued)

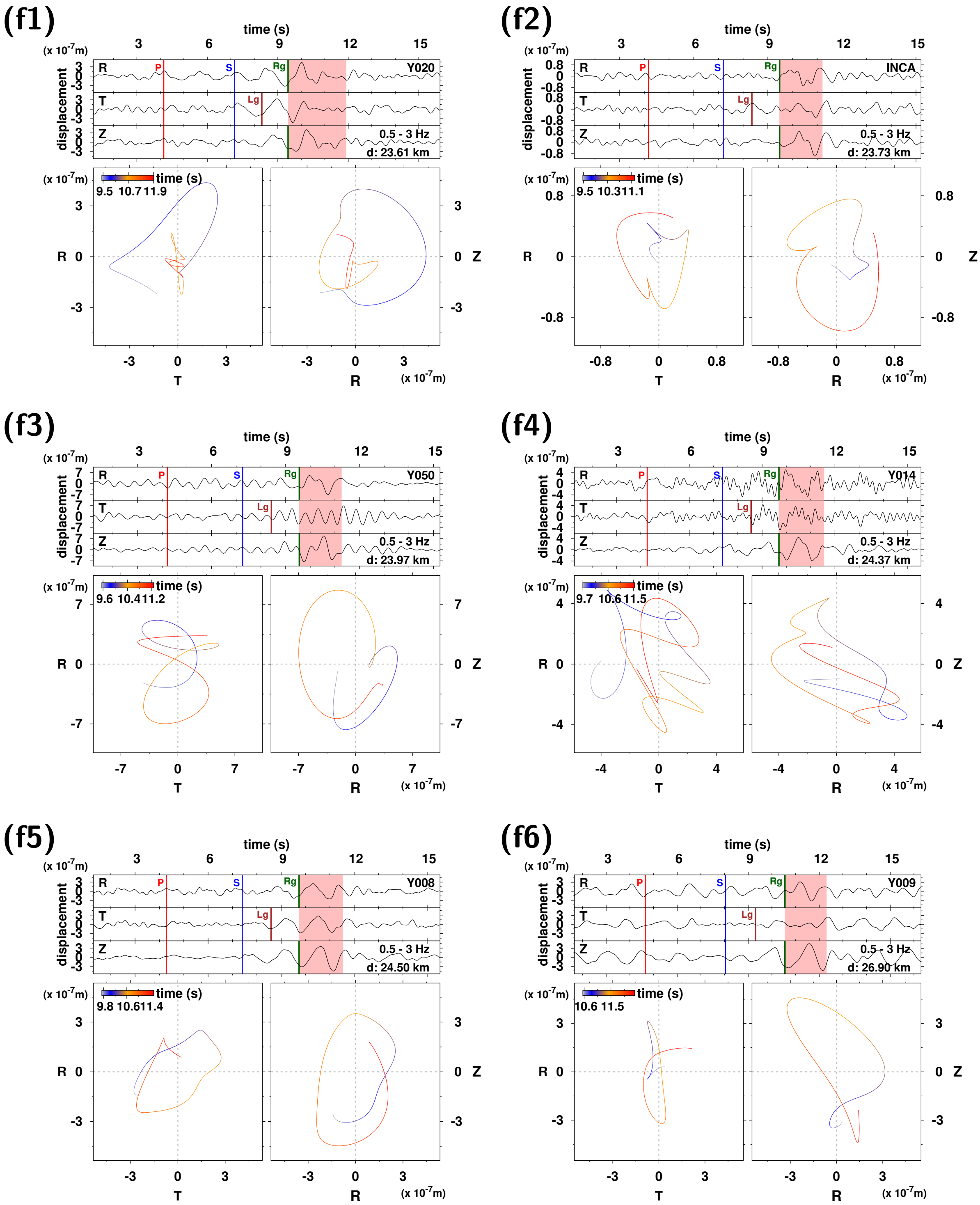

Figure S4. (continued)

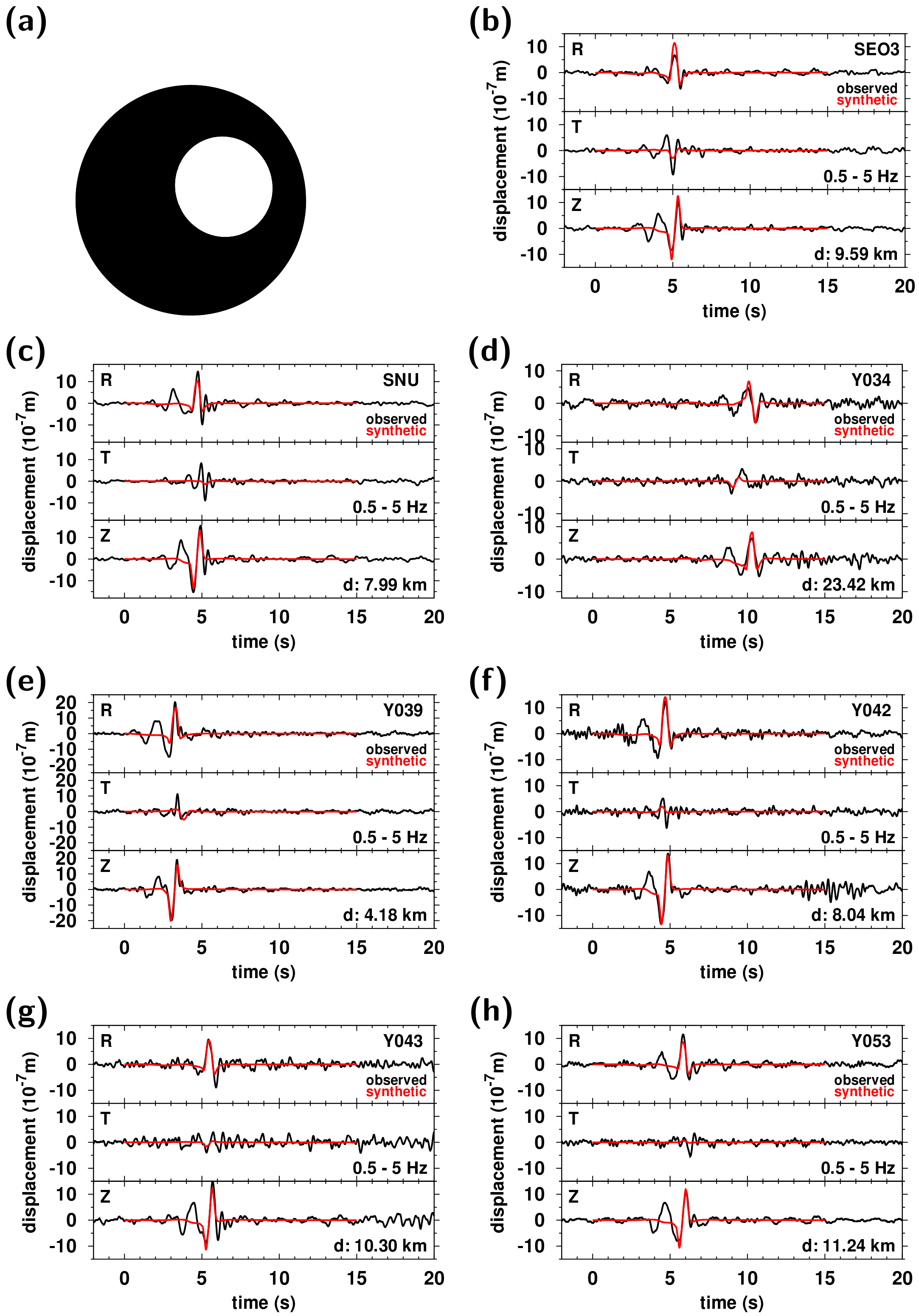

Figure S5. Modeling of seismic waveforms based on a normal-mode summation method for the second collapse stage: (a) the source mechanism, and waveforms at stations (b) SEO3, (c) SNU, (d) YO34, (e) Y039, (f) Y042, (g) Y045, and (h) Y053 are presented. The distances (d) are indicated. The synthetic waveforms agree well with the observed waveforms for the second collapse stage.

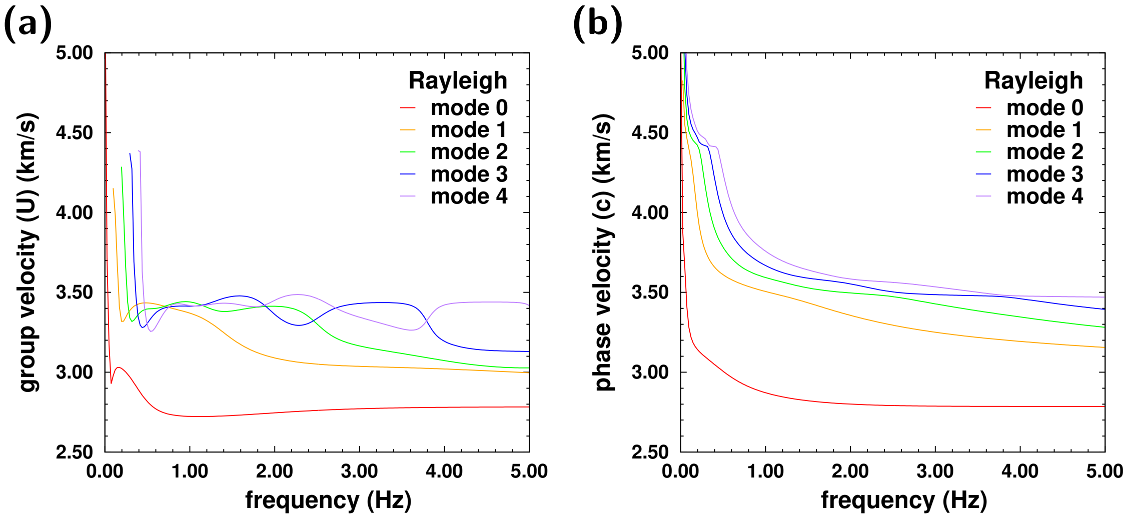

Figure S6. (a) Group- and (b) phase-velocity dispersion curves for Rayleigh waves in frequencies ≤ 5 Hz.

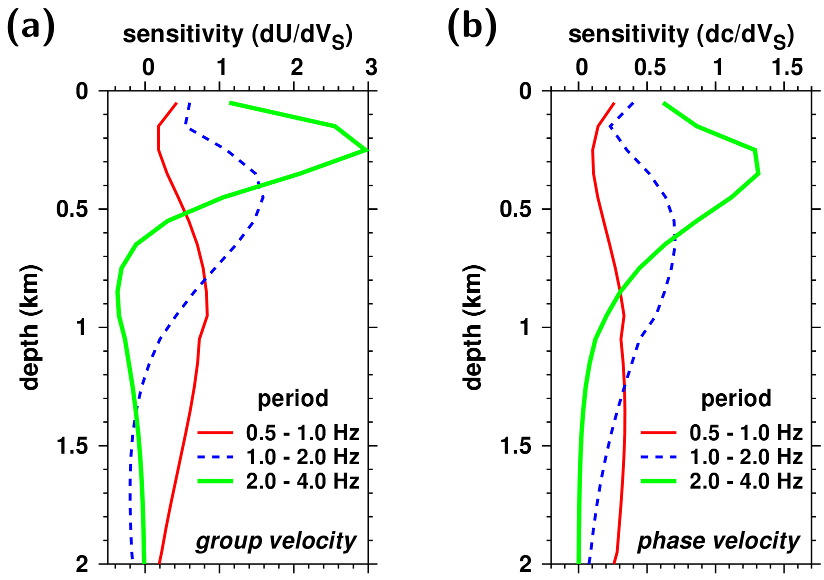

Figure S7. Sensitivity kernels of fundamental-mode Rayleigh waves for (a) group and (b) phase velocities. High-frequency waves are sensitive to changes in shallow media.

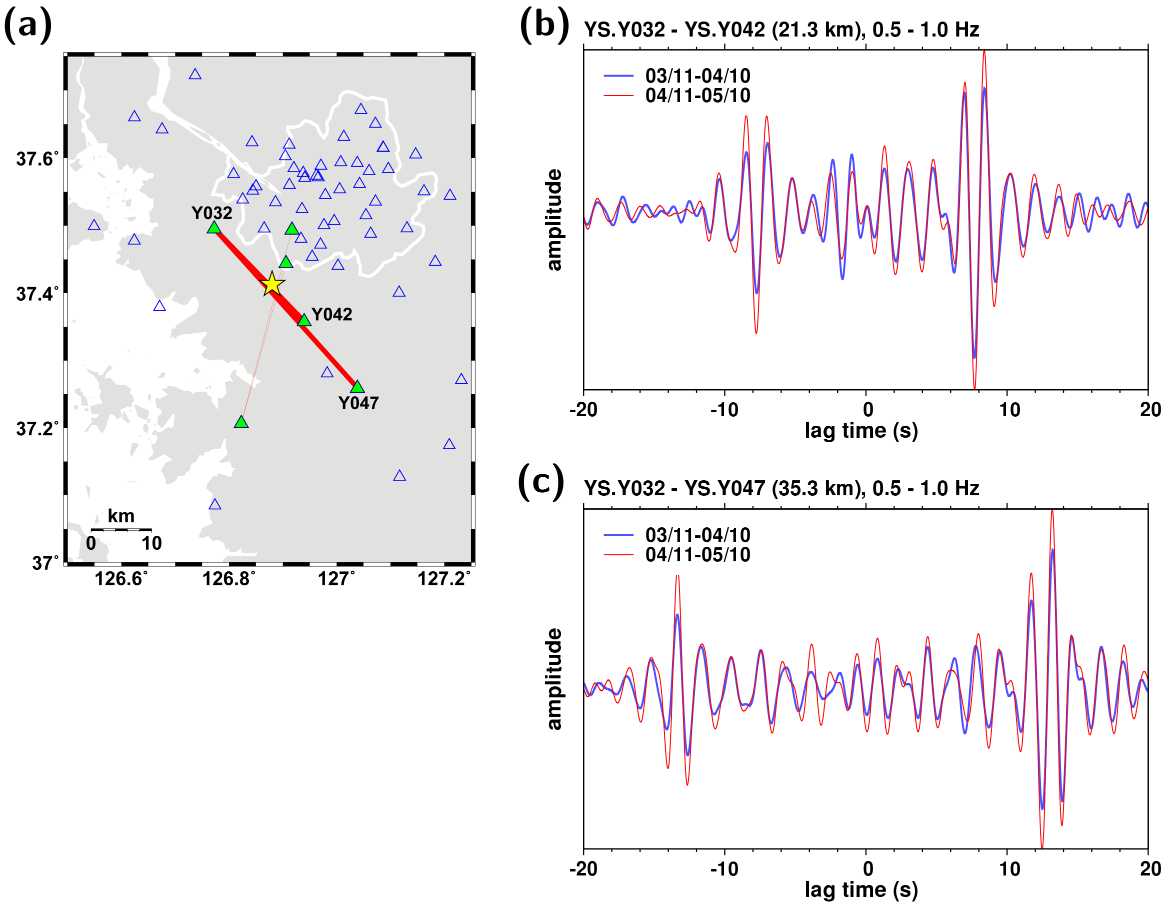

Figure S8. (a) Map of interstation paths in NW-SE across the sinkhole site, and one-month ambient-noise cross-correlation functions for interstation paths (b) Y032-Y042 and (c) Y032-Y047 in frequencies of 0.5-1.0 Hz. The ambient-noise cross-correlation functions are calculated for one-month before (March 11, 2025 to April 10, 2025) and after (April 11, 2025 to May 10, 2025) the sinkhole event. The ambient-noise cross-correlation functions present mild differences in phases.

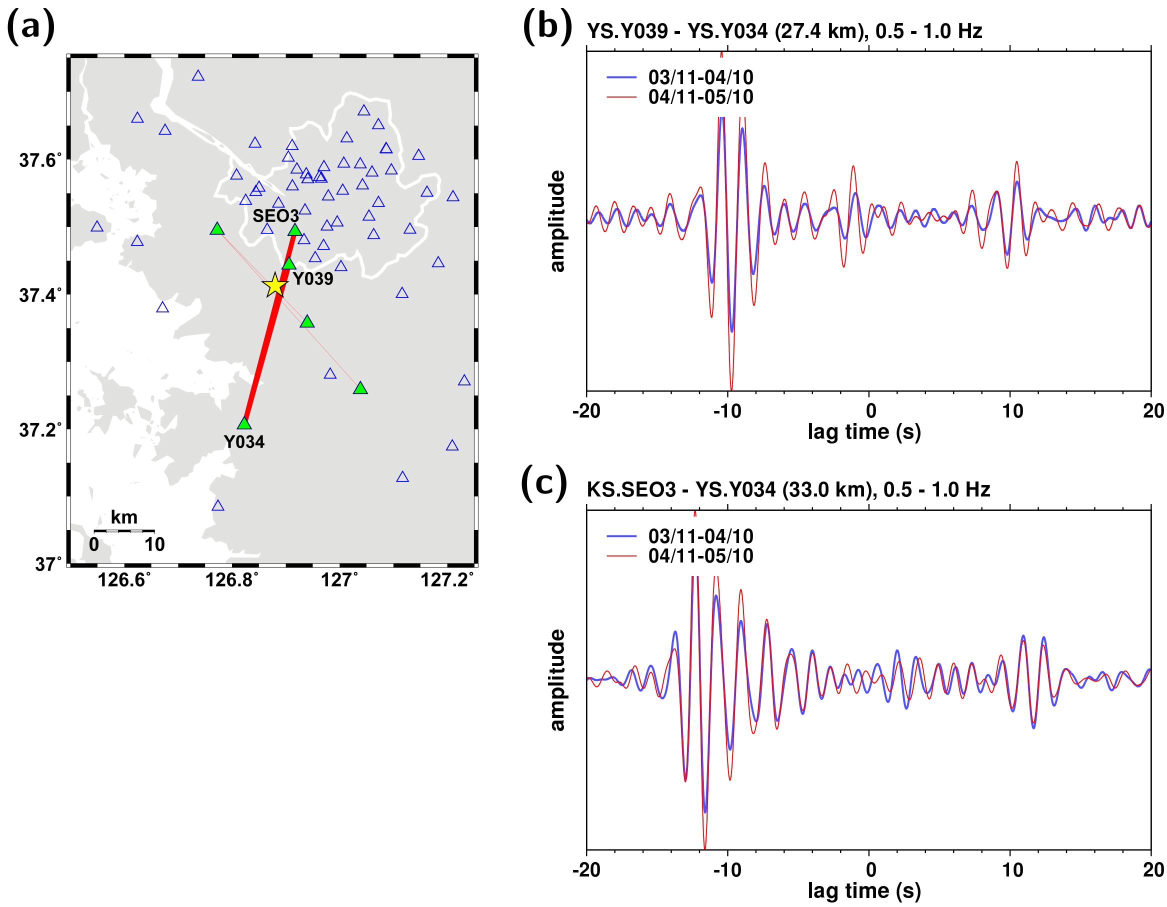

Figure S9. (a) Map of interstation paths in NE-SW across the sinkhole site, and one-month ambient-noise cross-correlation functions for interstation paths (b) Y039-Y034 and (c) SEO3-Y034 in frequencies of 0.5-1.0 Hz. The ambient-noise cross-correlation functions are calculated for one-month before (March 11, 2025 to April 10, 2025) and after (April 11, 2025 to May 10, 2025) the sinkhole event. The ambient-noise cross-correlation functions present mild differences in phases.

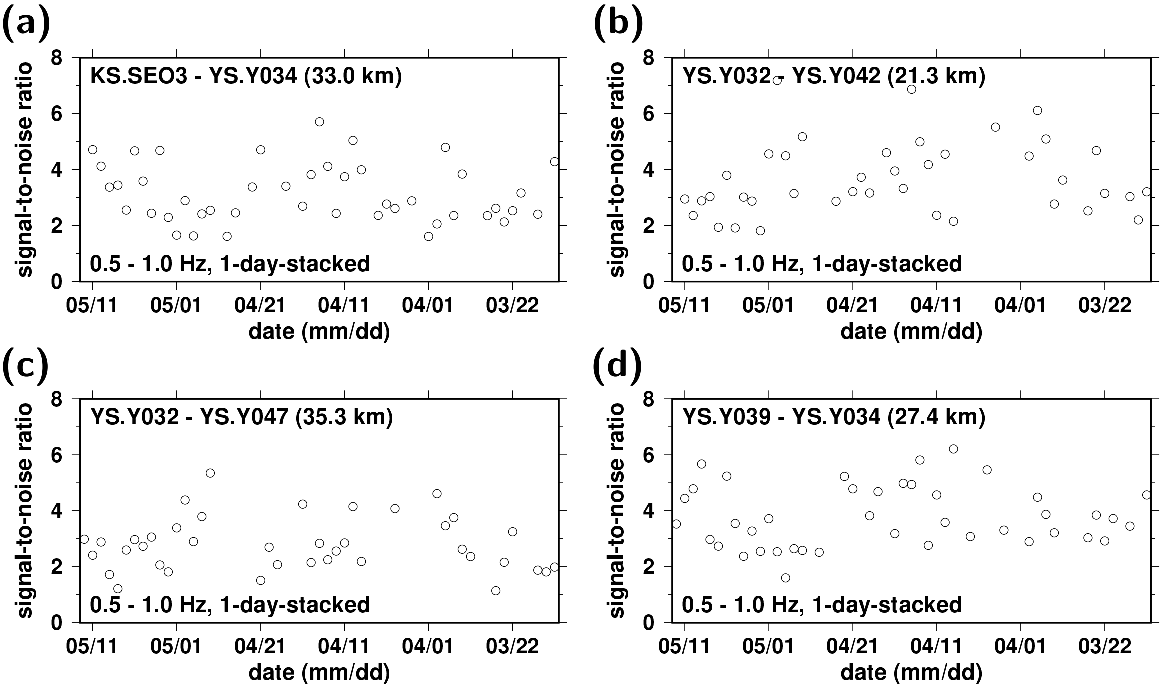

Figure S10. Signal-to-noise ratios (SNRs) of daily stacked ambient-noise cross-correlation functions in frequencies of 0.5-1.0 Hz for four station pairs: (a) SEO3-Y034, (b) Y032-Y042, (c) Y032-Y047, and (d) Y039-Y034. The signal amplitude is calculated as the zero-to-peak amplitude within the lag-time window of -20 to 20 s. The noise amplitude is calculated as the average zero-to-peak amplitude within the lag-time windows of -100 to -80 s and 80 to 100 s. The SNR varies with time and generally ranges from 2 to 6.

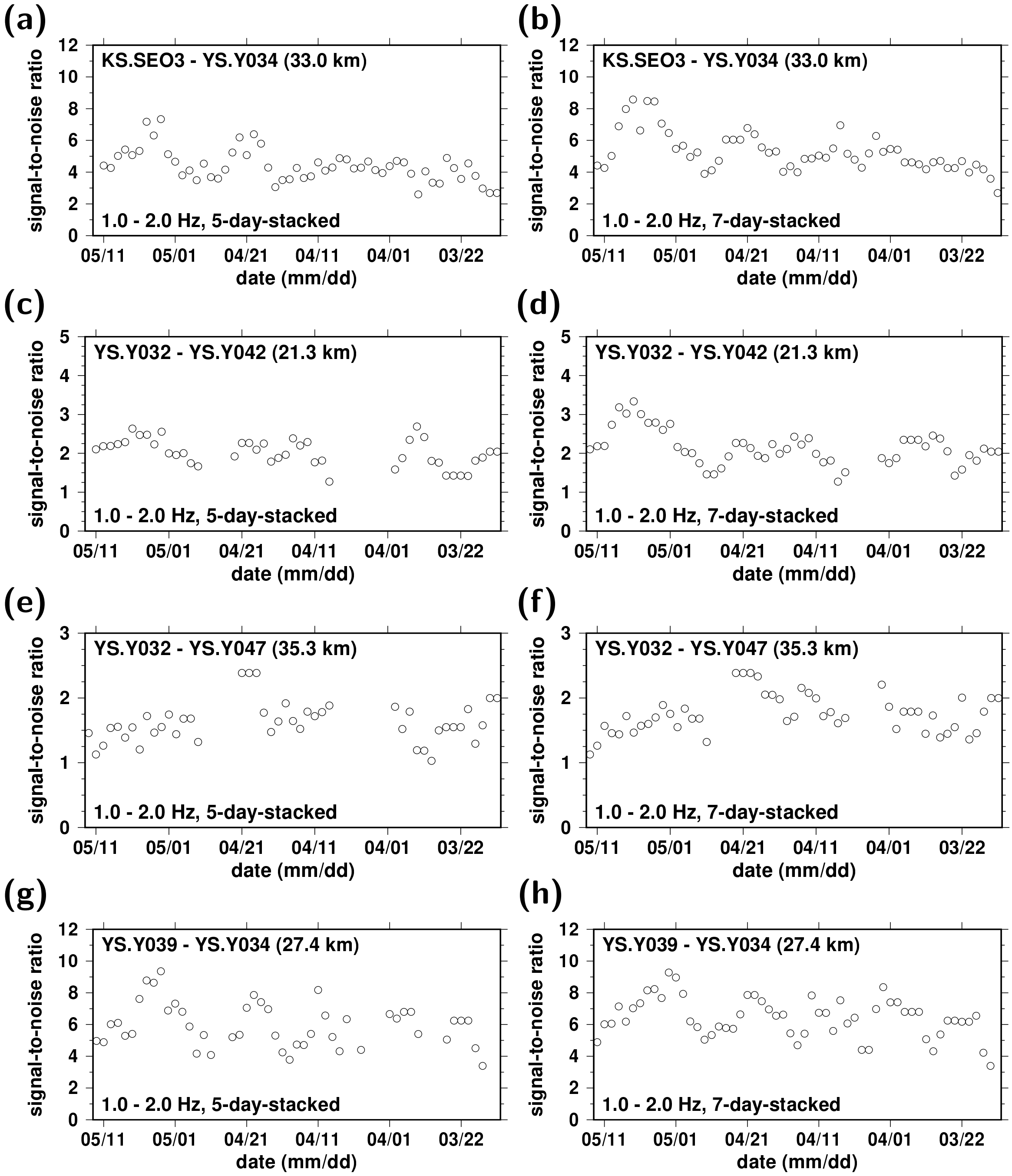

Figure S11. Signal-to-noise ratios (SNRs) of 5-day and 7-day stacked ambient-noise cross-correlation functions in frequencies of 1.0-2.0 Hz for four station pairs: (a) 5-day stacking for SEO3-Y034, (b) 7-day stacking for SEO3-Y034, (c) 5-day stacking for Y032-Y042, (d) 7-day stacking for Y032-Y042, (e) 5-day stacking for Y032-Y047, (f) 7-day stacking for Y032-Y047, (g) 5-day stacking for Y039-Y034, and (h) 7-day stacking for Y039-Y034. The comparison shows that the 7-day stacking analysis yields more stable cross-correlation functions and consistently higher signal-to-noise ratios than the 5-day stacking analysis.

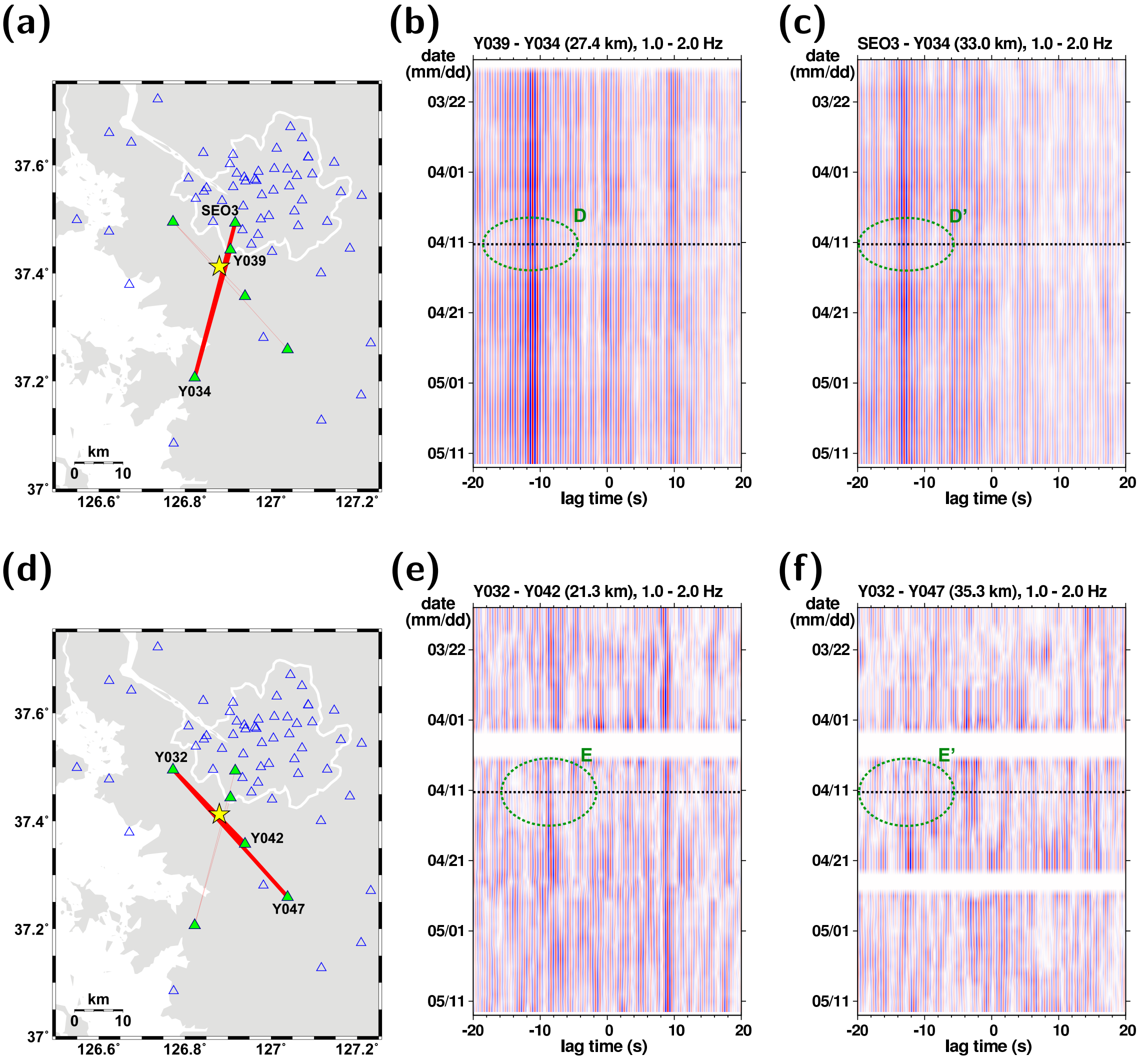

Figure S12. Daily variation of 7-day-stacked ambient-noise cross-correlation functions in frequencies of 1.0-2.0 Hz: (a) map of interstation paths in NE-SW, and results for paths (b) Y039-Y034 and (c) SEO3-Y034, and (d) map of interstation paths in NW-SE, and results for paths (e) Y032-Y042, and (f) Y032-Y047. Crosscorrelation functions for one day are stacked. Stable Green's functions are retrieved. The timing of sinkhole event is indicated (dotted line). Weak changes in Green's functions are observed (D, D', E, and E').

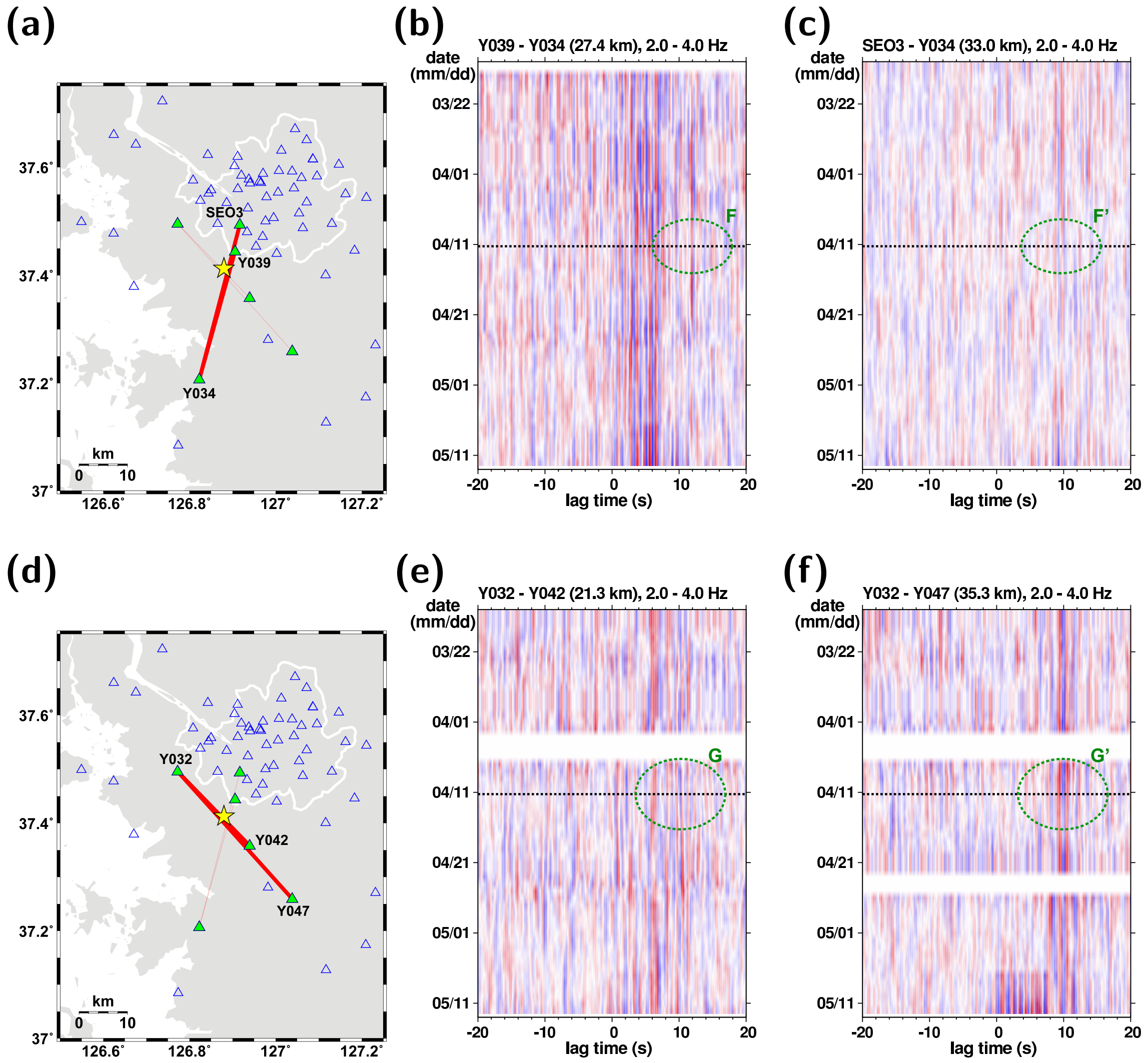

Figure S13. Daily variation of 7-day-stacked ambient-noise cross-correlation functions in frequencies of 2.0-4.0 Hz: (a) map of interstation paths in NE-SW, and results for paths (b) Y039-Y034 and (c) SEO3-Y034, and (d) map of interstation paths in NW-SE, and results for paths (e) Y032-Y042, and (f) Y032-Y047. Crosscorrelation functions for one day are stacked. Stable Green's functions are retrieved. The timing of sinkhole event is indicated (dotted line). Weak changes in Green's functions are observed (F, F', G, and G').